



MIT Open Access Articles

Simulation of polar ozone depletion: An update

The MIT Faculty has made this article openly available. **Please share** how this access benefits you. Your story matters.

Citation	Solomon, Susan, Doug Kinnison, Justin Bandoro, and Rolando Garcia. "Simulation of Polar Ozone Depletion: An Update." <i>J. Geophys. Res. Atmos.</i> 120, no. 15 (August 6, 2015): 7958-7974.
As Published	http://dx.doi.org/10.1002/2015JD023365
Publisher	American Geophysical Union (AGU)/Wiley
Version	Final published version
Citable link	http://hdl.handle.net/1721.1/103936
Terms of Use	Article is made available in accordance with the publisher's policy and may be subject to US copyright law. Please refer to the publisher's site for terms of use.

Journal of Geophysical Research: Atmospheres

RESEARCH ARTICLE

10.1002/2015JD023365

Key Points:

- Ozone loss chemistry strongly depends on polar stratospheric clouds and temperatures below 192 K
- ClONO₂ and HCl seasonal changes and variability are key indicators of chemistry
- Transport of ClONO₂ from the edge of the vortex to higher latitudes affects ozone loss

Supporting Information:

- Figures S1–S5

Correspondence to:

S. Solomon,
solos@mit.edu

Citation:

Solomon, S., D. Kinnison, J. Bandoro, and R. Garcia (2015), Simulation of polar ozone depletion: An update, *J. Geophys. Res. Atmos.*, 120, doi:10.1002/2015JD023365.

Received 13 MAR 2015

Accepted 24 JUN 2015

Accepted article online 26 JUN 2015

Simulation of polar ozone depletion: An update

Susan Solomon¹, Doug Kinnison², Justin Bandoro¹, and Rolando Garcia²

¹Department of Earth, Atmospheric, and Planetary Sciences, Massachusetts Institute of Technology, Cambridge, Massachusetts, USA, ²Atmospheric Chemistry Division, National Center for Atmospheric Research, Boulder, Colorado, USA

Abstract We evaluate polar ozone depletion chemistry using the specified dynamics version of the Whole Atmosphere Community Climate Model for the year 2011. We find that total ozone depletion in both hemispheres is dependent on cold temperatures (below 192 K) and associated heterogeneous chemistry on polar stratospheric cloud particles. Reactions limited to warmer temperatures above 192 K, or on binary liquid aerosols, yield little modeled polar ozone depletion in either hemisphere. An imposed factor of three enhancement in stratospheric sulfate increases ozone loss by up to 20 Dobson unit (DU) in the Antarctic and 15 DU in the Arctic in this model. Such enhanced sulfate loads are similar to those observed following recent relatively small volcanic eruptions since 2005 and imply impacts on the search for polar ozone recovery. Ozone losses are strongly sensitive to temperature, with a test case cooler by 2 K producing as much as 30 DU additional ozone loss in the Antarctic and 40 DU in the Arctic. A new finding of this paper is the use of the temporal behavior and variability of ClONO₂ and HCl as indicators of the efficacy of heterogeneous chemistry. Transport of ClONO₂ from the southern subpolar regions near 55–65°S to higher latitudes near 65–75°S provides a flux of NO_x from more sunlit latitudes to the edge of the vortex and is important for ozone loss in this model. Comparisons between modeled and observed total column and profile ozone perturbations, ClONO₂ abundances, and the rate of change of HCl bolster confidence in these conclusions.

1. Introduction

The discovery and explanation of the Antarctic ozone hole prompted field, laboratory, and modeling studies that rewrote much of the understanding of stratospheric chemistry and ozone depletion, largely during the 1980s. The fundamental connections between chlorofluorocarbon emissions, heterogeneous chemistry on stratospheric particles, and ozone depletion have been clear for decades [see Solomon *et al.*, 1986; Solomon, 1999, and references therein], but several new developments in stratospheric science motivate the current update.

First, field and laboratory studies have provided new data on the spatial and temporal distributions of both liquid and solid stratospheric particles, as well as their composition, size distributions, and chemical reactivities. While it has long been known that supercooled liquid sulfuric acid or solid (nitric acid trihydrate as well as water ice) polar stratospheric clouds (PSCs) could drive heterogeneous chemistry [e.g., Jet Propulsion Laboratory *JPL*, 2011, and references therein], the different particles were not initially thought to coexist. Recent satellite data showed that both liquid and solid PSC particles are present throughout the polar winter over much of the vortex, even under the extremely cold conditions of the Antarctic [Pitts *et al.*, 2009, 2013], consistent with developments in microphysical understanding and earlier local data [Biele *et al.*, 2001; Koop *et al.*, 1995; Peter and Grooß, 2012]. A surprisingly limited number of very large particles of nitric acid trihydrate particles were found under some conditions [Fahey *et al.*, 2001]. Because these particles are so large, they have less surface area and hence drive heterogeneous chemistry less efficiently than an equal mass of small particles; however, their sedimentation provides denitrification, which in turn influences ozone depletion [e.g., Toon *et al.*, 1986; Waibel *et al.*, 1999; Feng *et al.*, 2011]. These and other observations have stimulated examination of the chemical roles of different kinds of particles for chlorine chemistry and ozone depletion [e.g., the study by Wohltmann *et al.*, 2013, for Arctic conditions in midwinter in 2009–2010]. In this paper, we consider both hemispheres over the full depletion season.

Second, stratospheric modeling has progressed with the availability of state-of-the-art global stratospheric chemical models that have been subject to rigorous testing and intercomparison [e.g., Eyring *et al.*, 2010]. Some current global models can be driven with temperature fields from reanalysis data, and one such model is employed in this work. The reanalysis data have themselves become far more accurate in the

past few years due to improvements in bias corrections to the underlying data sets and in assimilation techniques [e.g., Rienecker *et al.*, 2011], although absolute stratospheric temperatures remain subject to uncertainties of the order of 2 K. The heterogeneous chemistry that drives ozone loss is strongly temperature sensitive, with just a degree or two of temperature difference causing large changes in reactivity and surface areas [e.g., Hanson *et al.*, 1994]. Therefore, testing the ability of a state-of-the-art global model driven with reanalyzed meteorological data to simulate the evolution of ozone is timely. We present results from a series of calculations for the year 2011. In 2011, unusually low temperatures and correspondingly anomalously large ozone losses occurred in the Arctic spring [Manney *et al.*, 2011; Sinnhuber *et al.*, 2011; Kuttippurath *et al.*, 2012], while 2011 Antarctic temperatures and ozone losses were similar to those in a number of other years in the past decade.

A third motivation for this paper is the observation of enhancements in stratospheric sulfate particles linked to a series of relatively small volcanic eruptions since about 2005 [Vernier *et al.*, 2011; Ridley *et al.*, 2014, and references therein]. These eruptions have episodically increased stratospheric aerosol loads observed in many regions by factors of several at numerous times in the past decade. While larger eruptions such as Pinatubo in the early 1990s have long been known to increase PSC surface area (by more than an order of magnitude for that eruption) and thereby increase polar ozone loss [e.g., Deshler *et al.*, 1994; Portmann *et al.*, 1996; Bregman *et al.*, 1997], whether smaller volcanic enhancements in stratospheric sulfate aerosol abundances could have had some influence on polar ozone depletion received less attention. Understanding of ozone recovery requires a detailed and quantitative attribution of decadal trends, and small factors [e.g., order 10 Dobson unit (DU) changes] can hence be important. In this study, we do not attempt to examine sulfate aerosol changes on a year-by-year basis. Rather, we examine a simple case in which a factor of three increase in sulfate aerosol densities (comparable to recent eruptions in the northern hemisphere) [see Ridley *et al.*, 2014] is imposed as an illustrative test.

The next section describes the model used, and section 3 discusses chemical considerations and the model test cases to be examined. Results are presented in section 4, and our conclusions are summarized in section 5. A supplement provides additional supporting information.

2. Model Description

The Community Earth System Model, version 1 (CESM1), is a coupled climate model for simulating the Earth's climate system. CESM1 is composed of four separate component models simultaneously simulating the Earth's atmosphere, ocean, land surface, and sea ice, and one central coupler component. The atmospheric component used in this study is the Whole Atmosphere Community Climate Model, version 4 (WACCM4), a comprehensive numerical model that spans the range of altitude from the Earth's surface to the lower thermosphere. WACCM4 is a superset of the Community Atmospheric Model, version 4 (CAM4), and includes all of the physical parameterizations of that model [Neale *et al.*, 2013]. WACCM4 is a fully coupled state-of-the-art interactive chemistry climate model; detailed intercomparisons between this model and others, as well as comparisons to a wide range of observations, have been reported in Eyring *et al.* [2010] and Marsh *et al.* [2013]. We use the specified dynamics version of WACCM4 (SD-WACCM), which is nudged to externally specified dynamical fields for temperature, zonal and meridional winds, and surface pressure fields from the Modern Era Retrospective Analysis for Research and Applications (MERRA) [see Rienecker *et al.*, 2011; also Lamarque *et al.*, 2012; Kunz *et al.*, 2011]. The chemical scheme includes the O_x , NO_x , HO_x , ClO_x , and BrO_x chemical families, along with gas phase and heterogeneous reactions on liquid binary and ternary sulfate polar stratospheric cloud particles, as well as solid nitric acid trihydrate and water ice polar stratospheric particles [Jet Propulsion Laboratory JPL, 2011]. Reactivities used for heterogeneous reactions are presented in Table 1, where a few minor exceptions from the kinetic recommendations presented in Jet Propulsion Laboratory JPL [2011] are noted.

The treatment of PSCs largely follows the methodology discussed in Considine *et al.* [2000] and Kinnison *et al.* [2007], plus updates discussed in Wegner *et al.* [2013]. This approach ensures that both liquid and solid particles are present even under extreme cold temperatures in Antarctic winter. At model temperatures above ~200 K, liquid binary sulfate (LBS) is the only aerosol represented. The LBS surface area density (SAD) used in the derivation of heterogeneous reaction rates is taken directly from the Chemistry Climate Model Initiative (CCMI) sulfate aerosol time series [Arfeuille *et al.*, 2013]. As the model atmosphere cools below 200 K, LBS

Reactions	NAT ^a	ICE ^a	Liquid Aerosols
$\text{N}_2\text{O}_5 + \text{H}_2\text{O}$	0.0004	0.02	~0.1
$\text{ClONO}_2 + \text{H}_2\text{O}$	0.004	0.3	<i>Shi et al. (2001)</i>
$\text{ClONO}_2 + \text{HCl}$	0.2	0.3	<i>Shi et al. (2001)</i>
$\text{HOCl} + \text{HCl}$	0.1	0.2	<i>Shi et al. (2001)</i>
$\text{BrONO}_2 + \text{H}_2\text{O}$	0.006 ^b	0.3 ^c	<i>Hanson et al. (1996)</i>
$\text{HOBr} + \text{HCl}$	–	0.3	<i>Hanson (2003)</i>

^aConsistent with JPL10-6 except where noted.^bDavies et al. [2002].^cListed as >0.2 in JPL10-6.

aerosols swell, taking up HNO_3 and H_2O to give supercooled ternary solutions (STS). The WACCM Aerosol Physical Chemistry Model (APCM) is used to derive the STS composition [Tabazadeh et al., 1994b]. The H_2SO_4 abundance used in APCM is derived from the observed sulfate SAD in the CCM1 data set for the simulations presented here. Nitric acid trihydrate (NAT) solid particles are also allowed to form. Observations [e.g., Peter et al., 1991] suggest that a

supersaturation of HNO_3 over NAT is needed before NAT can form. In all simulations in this study, the formation of NAT is assumed to occur at a supersaturation of 10, about 3 K below its thermodynamic equilibrium temperature [Hanson and Mauersberger, 1988]. The SAD and radius for STS and NAT assume a lognormal size distribution with a width of 1.6. In all but one simulation discussed in this work, the number of particles cm^{-3} is set to 10 and 0.01 for STS and NAT, respectively (Table 2). Wegner et al. [2013] added an additional constraint to the STS and NAT microphysical approach, where 20% of the total available HNO_3 is allowed to form NAT; the remaining 80% is available for STS. This essentially defines a nucleation approach consistent with a “mix 2” PSC representation as described in Pitts et al. [2009]. Following this approach yields gas-phase Antarctic HNO_3 abundances that compare well to Aura Microwave Limb Sounder (MLS) observations, suggesting that the denitrification scheme is realistic, although results compare less well to observations in the Arctic (see below). In this paper, we compare model composition results to level 2, version 3-3 MLS data, Michelson Interferometer for Passive Atmospheric Sounding (MIPAS) version 5 (R-ClONO₂_220), and ACE version 3.5 data. Figure S1 of the supporting information compares H_2O and HNO_3 values from the model to MLS measurements at several representative locations; see also Wegner et al. [2013].

The current microphysics package in SD-WACCM represents an equilibrium state for particle composition at a given temperature and available condensate distribution, but much research has shown that PSC particle microphysics is dependent on air parcel histories—i.e., whether cooling is rapid or slow [e.g., Meilinger et al., 1995; Larsen et al., 1997].

Table 2. SD-WACCM/MERRA Simulations for Year 2011

Scenario Name	Temperature Adjustment or Limit	PSC Types ^a	Comments ^{b,c,d}
NoHET	–	None	Halogen heterogeneous rates were zeroed.
REF	–	LBS, STS, ICE, NAT	Standard CCM1 REF1SD simulation.
REF –2Kbias	–2 K	LBS, STS, ICE, NAT	Temperature adjustment was applied to the derivation of SAD and heterogeneous rates, and to denitrification processes. Dehydration was not modified.
REF 3xSAD	–	LBS, STS, ICE, NAT	Input CCM1 sulfate SAD was multiplied by three between 300 and 10 hPa, poleward of 50°N, S.
REFnat	–	LBS, STS, ICE, NAT ^e	Two size modes were assumed for NAT, with particle densities of 0.0001 and 5 particles cm^{-3} . Denitrification occurred using the effective radius from the small density mode. STS was set to 5 particles cm^{-3} .
SOLIDS#1	–	ICE, NAT	Halogen heterogeneous rates on liquid particles were zeroed.
LIQUIDS#1	$T \geq 195$ K	LBS	Temperature limit was applied to the derivation of SAD and heterogeneous rates.
LIQUIDS#2	$T \geq 192$ K	LBS, STS	Temperature limit was applied to the derivation of SAD and heterogeneous rates.
LIQUIDS#3	–	LBS, STS	No temperature limit applied.

^aLiquid binary sulfate (LBS) are not considered to be PSCs. However, LBS heterogeneous reactions do occur at all temperatures up to the point when the sulfate aerosol thermodynamic conditions are present for uptake of H_2O and HNO_3 ; at this point, LBS particles become supercooled ternary solution (STS) particles.

^bParticle densities for STS (LBS), ICE, and NAT were set to 10, 0.1, and 0.01 cm^{-3} , respectively (except as noted for REFnat).

^cDehydration and denitrification processes in all simulations occurred over the entire model temperature range.

^dThe heterogeneous approach for all the simulations in this study (except REFnat) is based on Wegner et al. [2013].

^eThe derived effective radius and SADs for the two particle densities assigned to NAT were assumed to have an equal partitioning of the available condensed phase HNO_3 .

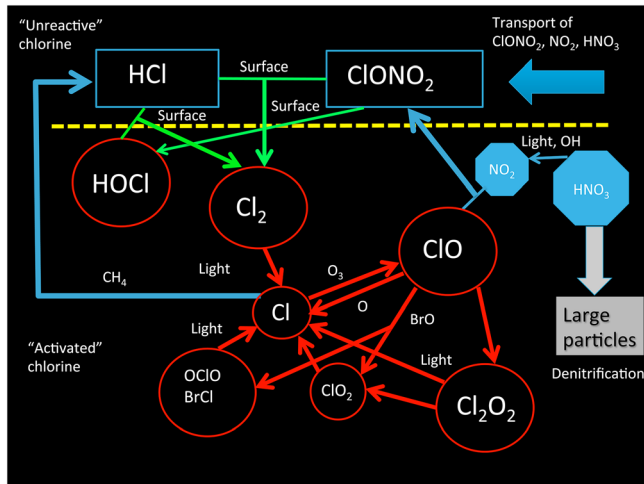


Figure 1. Schematic diagram of key chemical processes involved in polar ozone depletion. Unreactive chlorine is converted to active chlorine by heterogeneous processes on PSC surfaces denoted by green arrows. It is deactivated by processes and species denoted in blue. A yellow dashed line marks the distinction between unreactive and reactive chlorine.

As stated above, all but one of the tests presented in this paper constrain NAT to 0.01 particles cm^{-3} . A number of observations suggest that larger numbers of small NAT particles can sometimes occur in the real world [e.g., Tsias et al., 1999]. Detailed mechanisms of PSC formation remain uncertain, and a variety of relative abundances and mixes of particle types have been observed [e.g., Pitts et al., 2009, Pitts et al., 2013; Arnone et al., 2012; Hoyle et al., 2013; Achtert and Tesche, 2014]. If there were to be more NAT particles per unit volume, their effect on the chemistry would clearly be larger. We therefore carried out an additional test (Table 2, REFnat) in which two size distribution modes of NAT particles were imposed. This approach assumed 5 and 0.0001 particles cm^{-3} for the two

NAT modes. The amount of available condensed phase HNO_3 is divided evenly between the two modes. The total NAT SAD is the sum of the two modes and is used for derivation of heterogeneous reaction rates; the small number density mode is employed to derive the mean radius used in particle settling of condensed phase HNO_3 and therefore controls irreversible denitrification. To keep the total particle number density equal to $\sim 10 \text{ cm}^{-3}$, the number density of STS was reduced from 10 to 5 particles cm^{-3} . Water ice PSCs are also allowed to form. Here the underlying Community Atmospheric Model (CAM4) prognostic water approach derives and transports gas-phase, liquid-phase, and solid-phase water [Neale et al., 2010, 2013]. The solid-phase water (i.e., water ice) is settled at the saturation condition of water vapor over ice, resulting in irreversible dehydration of the stratosphere. Following this approach, gas-phase water abundances compare well to Aura MLS observations, suggesting that the dehydration scheme is realistic (see Figure S1). As in NAT and STS, the derived solid-phase water is used to derive the water ice SAD by assuming a lognormal size distribution, with a width of 1.6. In this study, the water ice particle density was set to 0.1 particles cm^{-3} .

3. Chemical Considerations and Model Test Cases Considered

Figure 1 presents a schematic diagram of the primary heterogeneous and homogeneous chemical processes that drive the depletion of polar ozone in the lower stratosphere. Chlorine released from the decomposition of chlorofluorocarbons can form the relatively inert reservoirs, hydrochloric acid (HCl), and chlorine nitrate (ClONO_2). These species react heterogeneously on and within particles to produce much more active forms of chlorine, e.g., Cl_2 and HOCl . Thus, these heterogeneous processes (along with similar reactions involving HBr and BrONO_2) are capable of “activating” chlorine from the reservoirs. Insofar as the chlorine remains activated, rapid ozone loss can occur through catalytic cycles in the sunlit atmosphere. While activation may take place during the dark polar winter, substantial ozone losses require the presence of sunlight as well as activated chlorine to drive the indicated catalytic cycles of ozone destruction shown in Figure 1 [e.g., Chipperfield et al., 1994]. Observations demonstrate that the bulk of Antarctic ozone loss occurs in the spring, when the polar cap is illuminated but still cold; Arctic ozone also displays the largest chemical depletion in spring rather than winter (see Figure 2 below).

Previous work has demonstrated that the competition between activation and deactivation is critical to ozone destruction [e.g., Portmann et al., 1996]. Deactivation proceeds more and more rapidly as the polar spring advances, in part because returning sunlight produces NO_2 from HNO_3 , which in turn forms ClONO_2 . If it is not cold enough for heterogeneous processing to activate ClONO_2 (and HCl) more rapidly than deactivation takes place, then active chlorine will be drained away into the reservoirs, and ozone depletion will be

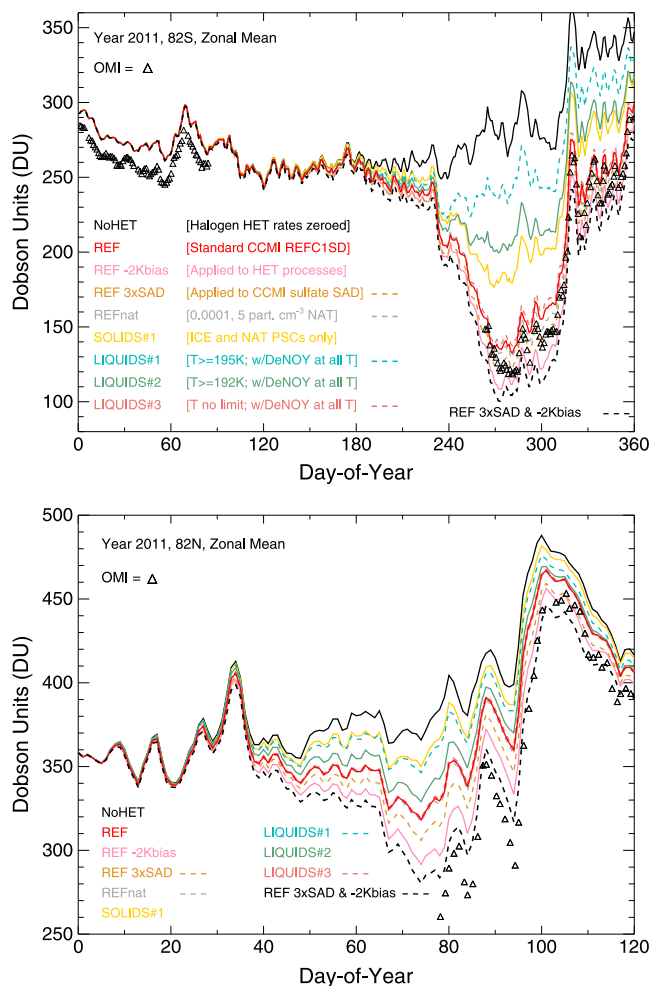


Figure 2. Seasonal evolution of model simulated zonally averaged total column ozone in 2011 in (top) Antarctica and (bottom) the Arctic at $\pm 82^{\circ}$ latitude in each hemisphere, for the series of tests of heterogeneous chemical processes described in detail in Table 2 (different colored lines). Corresponding observations from the OMI satellite record are also shown for comparison (triangles). OMI observations are only available for the sunlit portion of the year.

Chemical mechanisms will be discussed in more detail after presenting information on the behavior obtained in various model test cases. The test cases are presented in Table 2. These tests have been designed to illuminate the relationships of ozone depletion to the chemistry of liquid and solid stratospheric background and cloud particles, as well as the roles of small changes in temperature, and an imposed small-volcano-like enhancement in sulfate content. A run in which heterogeneous chlorine and bromine chemistry on all types of particles is turned off provides a baseline for calculation of chemical ozone depletion (but note that the surface reaction of $\text{N}_2\text{O}_5 + \text{H}_2\text{O} \rightarrow \text{HNO}_3$ is permitted in that case, since it does not directly involve chlorine or bromine).

4. Results

4.1. Total Ozone: Sensitivity to Liquid and Solid PSCs, Surface Area, and Temperature

Figure 2 presents the seasonal evolution of calculated zonally averaged total column ozone for various cases as simulated by WACCM for 2011, in the Antarctic at 82°S and in the Arctic at 82°N . The figure also shows the column abundances observed by the Ozone Monitoring Instrument (OMI) in that year. Results here and elsewhere in this paper are zonal averages and do not depict the larger ozone losses seen locally in the

terminated. Except in the dark period of polar winter when little ozone loss occurs, it is insufficient to consider only activation of chlorine. Instead, the net of activation minus deactivation (referred to in this paper as net activation) must be evaluated if chlorine's relevance to ozone loss is to be understood.

Formation of PSC particles with sufficient size and mass to sediment can remove much of the reactive nitrogen (in the form of HNO_3) from the stratosphere, decreasing the amount of NO_2 available to form ClONO_2 . Therefore, the extent of such denitrification is a factor in ozone loss as well [Toon *et al.*, 1986; Feng *et al.*, 2011]. However, while denitrification can be very extensive (particularly under the very cold conditions that prevail in the Antarctic), some gas-phase HNO_3 will remain available, which can photolyze and deactivate chlorine as sunlight returns to the polar regions in spring. Deactivation into HCl is also important and is related to the ratio Cl/ClO and to NO densities (through their effects on the rate of $\text{Cl} + \text{CH}_4$ and $\text{OH} + \text{HCl}$) [see Douglass *et al.*, 1995], which in turn are linked to both temperatures and sunlight.

In summary, each spring there is a race that determines much of the polar ozone depletion, with the key factor being the competition between the ways that returning sunlight and related warming affect both the rates of ozone photochemistry and the net chlorine activation.

displaced Arctic vortex in 2011 [Manney *et al.*, 2011]; although these contribute to the zonal average, their contribution is diluted by smaller losses at other longitudes. The reference case (referred to in the figures as REF) including the model's standard formulation for liquid and solid PSCs (solid red curves) reproduces the observed seasonal decline of Antarctic column ozone decline very well. Along with the longer term changes over the season, short-term variations of the Antarctic ozone column over a few days are also captured with fidelity by SD-WACCM and largely reflect the planetary wave displacements of the polar vortex captured in the MERRA reanalysis. Comparison of zonal averaged chemical composition to observations (e.g., for ozone and HCl as shown in the figures) provides an important test of SD-WACCM's representation of important wave-induced changes in temperature, illumination, and transport.

Contrary to the behavior over Antarctica, the reference case of SD-WACCM underestimates Arctic ozone depletion. Brakebusch *et al.* [2013] suggested that SD-WACCM using MERRA reanalysis was biased warm at some altitudes relative to MLS observations of temperature, by about 1–2 K in the Arctic, but it is not clear whether MERRA or MLS should be considered more authoritative given the limits to current measurement accuracy and precision. For the purposes of illustration, Figure 2 also shows how sensitive the heterogeneous chemistry would be to such a difference in temperature (solid pink curves). The potential 2 K bias is applied only to the heterogeneous chemical reactivities and the derivation of PSC surface area in these tests. Because of the strong temperature dependence of the heterogeneous chemistry (probed further below), a 2 K error in temperature affects Arctic ozone loss substantially (consistent with many earlier studies) [e.g., Van den Broek, 2000]. Sinnhuber *et al.* [2011] obtained an enhancement in simulated 2011 Arctic ozone column loss of 25 DU for a 1 K temperature perturbation, while Rex *et al.* [2004] inferred an observed sensitivity of 15 DU per 1 K perturbation based on an average of 10 years of Arctic data. Our Arctic 2011 value of about 40 DU for a 2 K perturbation is comparable. While not fully resolving the discrepancy, such a shift brings the results much closer to the observations. Figure 2 also illustrates the potential importance of changes in the sulfate aerosol abundance (such as those caused by volcanic eruptions) that provide the nuclei for PSCs. The dashed gold curves indicate a test case where both temperatures and sulfate are jointly changed. These tests support the view that PSC surface areas and reaction rates both matter to polar ozone losses, with small change in temperatures having a large effect [see Bregman *et al.*, 1997].

Two test runs were carried out to explore how much ozone losses depend on cold temperatures and PSCs. In these runs, both the heterogeneous chemical reactivities and particle surface areas were kept at their values for 195 K or 192 K even when temperatures became colder than these limits, while denitrification was kept the same as the reference case (see below). In the test run limiting heterogeneous chemistry to the rate for binary liquid particles at temperatures of 195 K even when temperatures become lower than that (LIQUIDS#1; dashed blue curves), almost no total column ozone loss is obtained in SD-WACCM in the Antarctic or Arctic. This result differs markedly from the results reported in Drdla and Mueller [2012, their Table 2], who state that reactions on liquid binary aerosols alone at temperatures no colder than 195 K are sufficient to account for the bulk of both Arctic and Antarctic ozone depletion. The second liquids-only test run limiting heterogeneous chemistry to the rate for liquid particles at temperatures of 192 K (LIQUIDS#2; solid green curves) also produced little column ozone loss in either polar region in SD-WACCM. Since denitrification is driven by solid particles, these tests including denitrification, but only allowing temperature-dependent heterogeneous chlorine and bromine chemistry to act on liquids, are not a realistic representation of what liquid particles alone can do but are presented for illustration. However, additional tests (not shown) indicate that little ozone loss is obtained in cases where liquid chemistry is limited to the rates at temperatures of 192 K or warmer irrespective of whether denitrification is included.

Below about 192 K, liquid stratospheric particles take up nitric acid and water, such that they swell and become ternary PSCs or supercooled ternary solutions [Carslaw *et al.*, 1994, Tabazadeh *et al.*, 1994a]. Such swelling greatly increases both reactivities and surface areas. Formation of PSCs is essential for substantial ozone losses in WACCM. A liquids-only case was run in which heterogeneous chemistry occurs at all temperatures, and liquid particles were allowed to swell to become liquid polar stratospheric clouds (LIQUIDS#3). Denitrification is included, but no solid particle chemistry is permitted in this case. This case yields ozone losses that are very close to the reference case in both Antarctica and in the Arctic, illustrating that liquid PSCs alone at sufficiently cold temperatures can drive much of the chemistry needed to rapidly deplete ozone, as has long been known [see, e.g., Portmann *et al.*, 1996; Ravishankara and Hanson, 1996; Carslaw *et al.*, 1997].

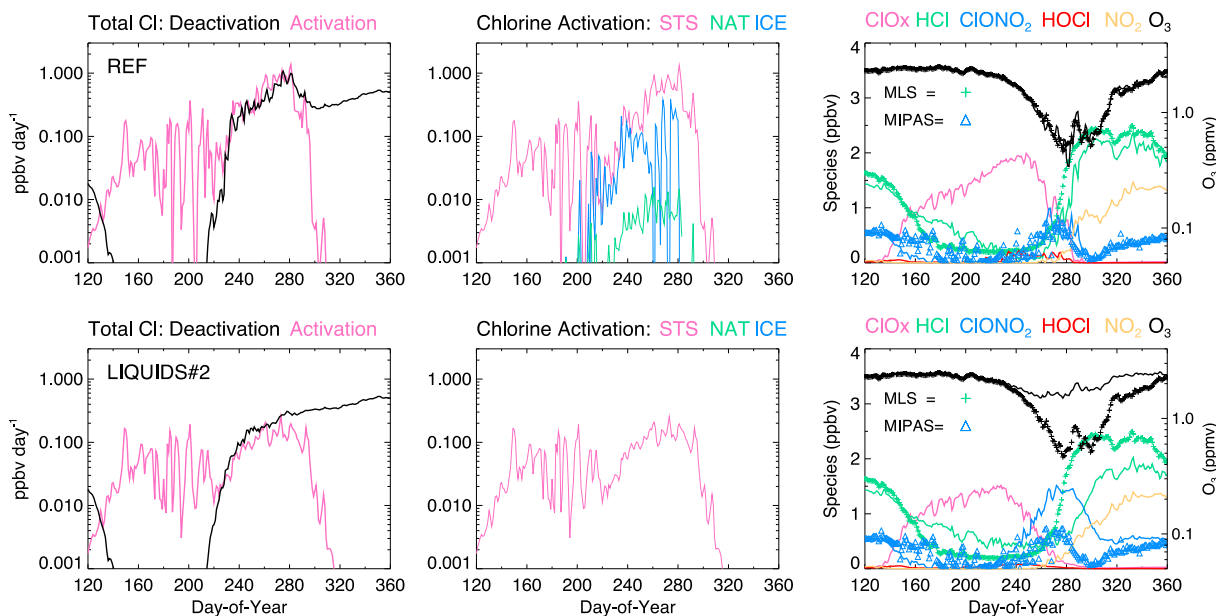


Figure 3. Key chemical processes and constituents at 74°S (zonally averaged), 61 hPa. Rates of activation of chlorine (driven by the heterogeneous reactions on liquid particles, NAT, and ice as in Table 1 and Figure 1) and rates of deactivation (through conversion to CIONO₂ and HCl; see Figure 1) are shown for the (top) reference and (bottom) LIQUIDS#2 cases. Concentrations of ozone, HCl, and CIONO₂ calculated by SD-WACCM (lines) are compared to MLS and MIPAS satellite data (crosses and triangles, respectively) in the right panels, where calculated abundances of related species are also indicated.

A test run including only the chemistry of solid PSC particles at all temperatures but neglecting the effects of liquid polar stratospheric clouds is also presented (SOLIDS#1; solid yellow curves). This case does not produce as much ozone loss as the reference or LIQUIDS#3 cases, but produces much more ozone loss than the LIQUIDS#1 or LIQUIDS#2 cases. It is important to note that Figure 2 shows that the depletions due to liquid or solid PSCs are not additive. For example, in Antarctica, about half as much ozone depletion as in the reference run is obtained when only solid particles are considered, but when only liquids are considered over the full range of temperatures, results are very close to those of the reference run. Thus, the reference run is not a sum of the two; rather liquid or solid PSCs can each drive substantial heterogeneous chemistry. Hence, such tests cannot determine specific percentages of ozone loss attributable to different types of PSCs in the real world, even if the simplified microphysics package of the model is assumed to be realistic (see further discussion below) and denitrification is included in all cases.

4.2. Ozone Chemistry and Profile Changes

We next further probe the chemistry occurring at illustrative sample pressure levels (upper, middle, and lower parts of the range of ozone-depleted altitudes) and latitudes (deep in the vortex, middle vortex, and outer vortex) in the Antarctic and Arctic; the results shown are not very sensitive to the exact choice of selected latitudes and pressure levels, and are broadly representative of the two regions.

As an example of key processes in Antarctic ozone depletion, Figure 3 shows how the zonally averaged seasonal ozone loss, activation, and deactivation evolve in SD-WACCM at 74°S near 60 hPa. MLS observations of ozone and HCl, as well as MIPAS observations of CIONO₂, are also plotted for comparison and will be explored further below. The figure illustrates the competition between activation and deactivation that occurs in the sunlit atmosphere and shows why the gross activation alone is not an appropriate measure of whether heterogeneous chemistry is fast enough to drive substantial ozone loss in sunlit air. Since deactivation rates grow rapidly as sunlight returns to the southern polar cap, fast activation after about day 250 is required at this location if net chlorine activation is to be positive and significant ozone losses are to occur.

Figure 3 also illustrates that both liquid PSCs and water ice make important contributions to the rate of chlorine activation at this location in the reference case, allowing the activation to outpace deactivation until about mid-September and driving substantial ozone loss. Transport processes also play a role along

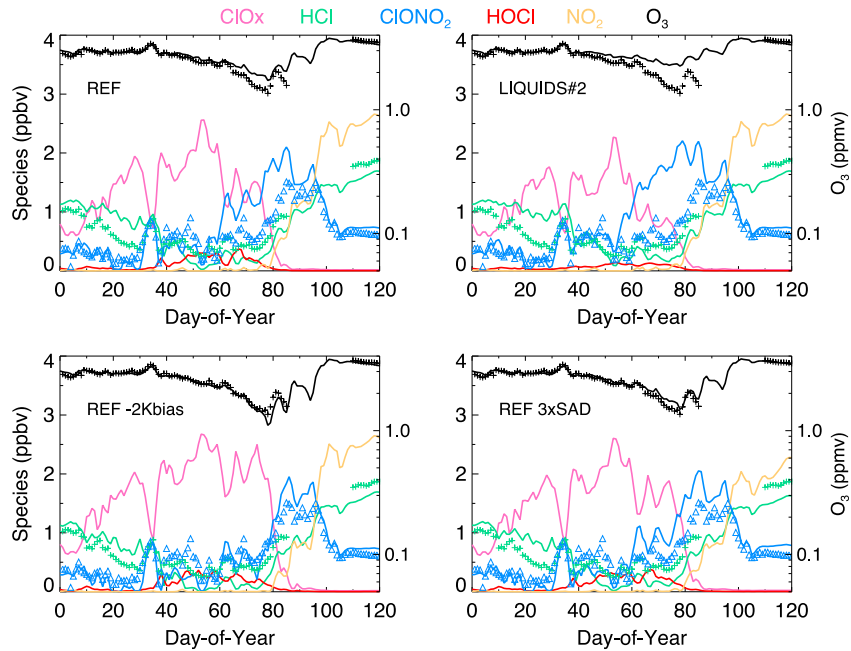


Figure 4. Evolution of chemical species at 82°N (zonally averaged) and 53 hPa. Concentrations of ozone, HCl, and CIONO₂ calculated by SD-WACCM (lines) are compared to MLS and MIPAS satellite data (crosses and triangles, respectively), and calculated abundances of related species are also indicated.

with chemistry as discussed further and shown in Figure 11 below. Temperatures at this location are well below 190 K through mid-September, and ice particle formation is to be expected given the observed amounts of water vapor (about 2.5 ppmv from MLS data, in good agreement with the SD-WACCM parameterization). However, if no water ice chemistry is permitted to occur, and heterogeneous chemistry acts only on liquid particles (over the full range of temperature), the net activation is very close to that found in the reference case and the ozone loss is nearly identical (see Figure S2). These tests illustrate that the net chlorine activation at this location is insensitive to the type of particle, so long as it is fast enough to keep up with the rate of supply of CIONO₂.

Figure 4 presents sample composition changes in the Arctic ozone depletion region at 82°N, near 60 hPa in SD-WACCM. The figure shows the evolution of ozone at this level for the reference, LIQUIDS#2 (heterogeneous chemistry at 192 K or warmer), REF -2Kbias, and REF 3xSAD cases compared to MLS data. Differences in ozone loss between the four cases are significant, illustrating the strong sensitivity of the chemistry here. Note that the re-emergence of CIONO₂ in spring differs significantly in the four cases shown; we return to this point below.

Overall, key findings of Figures 2–4 are (i) the importance of the competition between activation and deactivation, and (ii) the central role of heterogeneous PSC chemical processing in SD-WACCM at cold temperatures below 192 K. Changes in temperature of just 2 K can cause important increases in the ozone losses, especially in the Arctic. Just as temperatures are important, the results are also sensitive to changes in surface areas: in a test run including a factor of three increase in background sulfate aerosol concentration (as could occur following a relatively minor volcanic eruption), the total column ozone losses also increase significantly, emphasizing the importance of understanding sulfur input to the stratosphere.

Figure 5 explores the profile of ozone loss for the different chemical tests as ozone nears its 2011 seasonal minimum, day 270 (end of September) in Antarctica and day 80 (mid-March) in the Arctic. Figure 5 provides percent differences for each case compared to the run without heterogeneous chlorine and bromine chemistry; hence, this figure shows zonally averaged chemical ozone depletion. The height dependence of ozone loss is linked to both physical and chemical properties. At lower altitudes below about 80 hPa in the Arctic, temperatures are warmer than in the heart of the depletion region so that solid PSCs form infrequently and hence are not important in chemical processing. Further, the chlorine

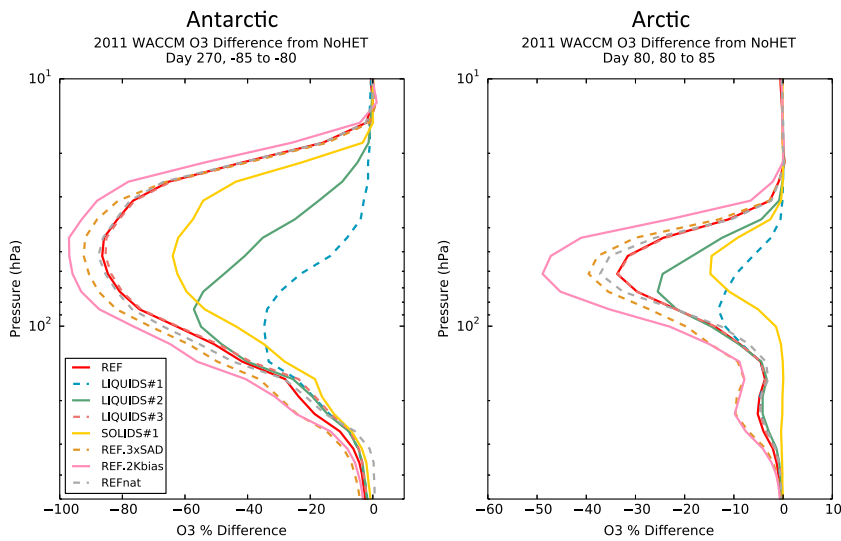


Figure 5. Ozone depletion profiles for various model cases, relative to NOHET in 2011. (left) Antarctic, average of 80°S to 85°S, day 270; (right) Arctic, average of 80°N to 85°N, day 80.

activation by liquid aerosols is highly sensitive not only to temperature but also to altitude, due to the effect of atmospheric pressure on the partial pressures of the available condensable gasses, H₂O, HNO₃, and H₂SO₄. The condensation of vapors causes liquid particles to swell, increasing both their surface areas and their reactivity through dilution with water so that the increase of pressure at lower altitudes enhances liquid activation [see, e.g., the review in Solomon, 1999, and references therein]. Conversely, at lower pressures (e.g., near 30–40 hPa), where liquid condensation becomes limited by lack of vapor, solid PSCs can play a relatively larger role whenever temperatures are low enough for them to form.

Figures 6 and 7 expand on the results of Figure 5 by showing the full seasonal development of the ozone losses at a range of pressure levels for selected test cases. The figures show the percent changes over time compared to days 220–230 in the Antarctic and days 1–10 in the Arctic, respectively, for both the data and model results. The figures also compare modeled seasonal changes of ozone with those observed by the Microwave Limb Sounder (MLS). At some altitudes and latitudes, where transport is limited compared to the rapid rate of depletion, ozone would remain fairly constant through the season in the absence of chlorine chemistry as shown by the NOHET curves in the figure so that the figures approximate ozone losses. For comparison, the supplementary material shows analogous time series relative to the case in which heterogeneous chlorine and bromine chemistry is turned off entirely, as in Figure 5. Although there are important differences in detail between Figures 6 and 7 and Figures S3 and S4 at some pressure levels (particularly at the edges of the depletion region below about 150 hPa and near 30 hPa), the similarities attest to the important role of heterogeneous chemical processing on PSCs at temperatures below 192 K in driving the seasonal decreases of ozone in Arctic and Antarctic spring in 2011 in SD-WACCM.

Figure 6 shows broad consistency between the modeled and observed seasonal evolution of the height-dependent ozone concentration decline in the heart of the polar region in Antarctica for the reference case. The largest Antarctic discrepancies occur at the lowest altitudes near 120 hPa, where one possible explanation is insufficient local sulfur content to drive the modeled supercooled ternary solution chemistry that is the dominant ozone loss process at this altitude (illustrated by the REF 3xSAD case). In the Arctic (Figure 7), the reference model does not agree as well with the observations as in the Antarctic, and tests shown here are consistent with the findings of Brakebusch *et al.* [2013] regarding a possible –2 K error in temperature. However, SD-WACCM still does not reproduce the observations near 30 hPa even in this case, suggesting possible shortcomings in the model chemistry. Because solid PSCs play a more important role at these altitudes than at lower levels, one possible explanation could be errors in solid PSC surface areas or their chemistry.

4.3. HCl and ClONO₂: Key Indicator Species

In this section, we show that the evolution of the HCl and ClONO₂ reservoirs after polar sunrise is a key indicator of heterogeneous processing. Figure 8 presents the modeled evolution of ozone along with HCl, ClONO₂, and

Antarctic

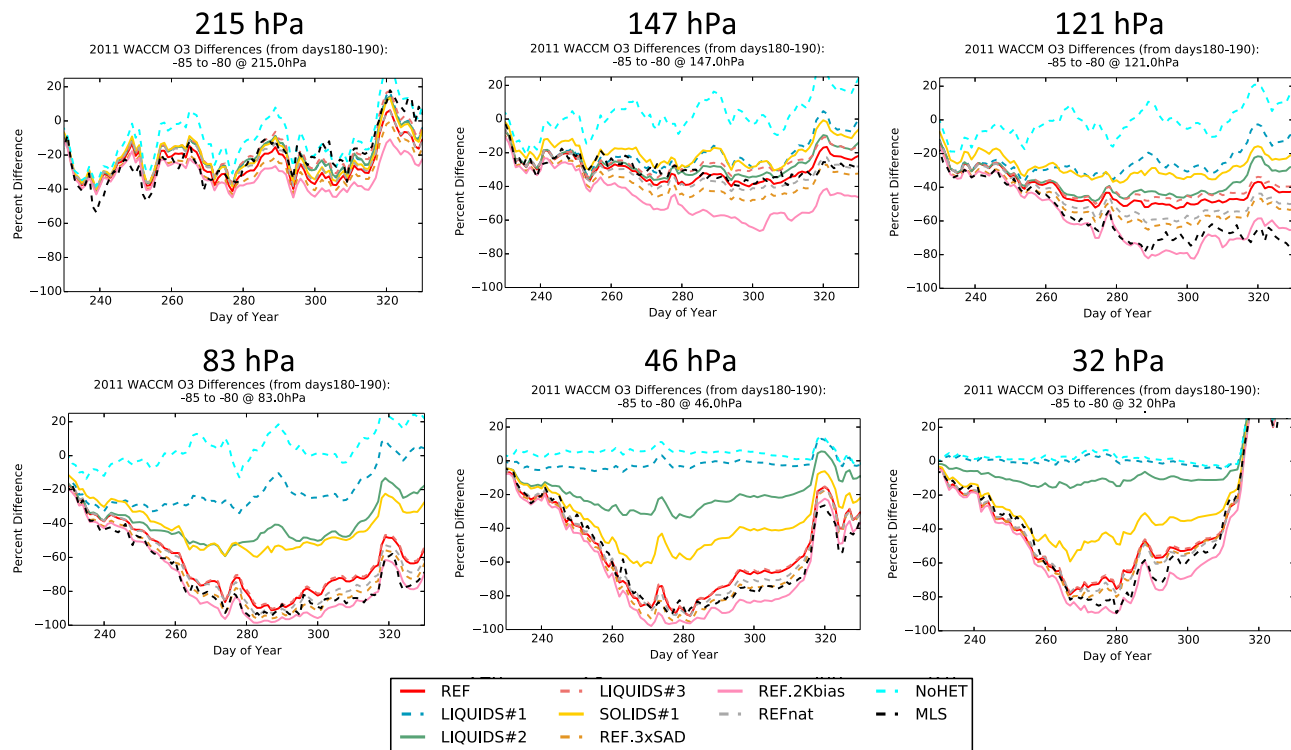


Figure 6. Seasonal evolution of percentage ozone changes at various pressure levels in the Antarctic, averaged over 80°S to 85°S, for various model cases compared to MLS data, relative to days 180–190 for each case.

several other species near 30 hPa at 80°S and 70°S, for the reference and LIQUIDS#2 (where heterogeneous chlorine and bromine reactions act only on liquids at temperatures above 192 K). The figure also includes MLS and MIPAS observations of ozone, HCl, and ClONO₂ for comparison.

The 30 hPa pressure level provides a sensitive test of key ozone loss chemistry, in part because of its high exposure to both sunlight and cold Antarctic temperatures. Further, it is well established that when ozone abundances drop to extreme low values (below a few tens of a pptv) at higher pressures near 50 or 70 hPa in the core of the vortex, formation of ClO (and hence ClONO₂ and HOCl) is impeded; rapid deactivation into HCl must then occur even if PSCs are still present and temperatures are very cold [Douglass *et al.*, 1995]. The 30 hPa level does not undergo such extreme ozone depletion, and this facilitates elucidation of the competition between deactivation and activation compared to other levels in the vortex core.

Figure 8 shows that the behavior of ClONO₂ is central to the large disparity in ozone loss between the reference case and the LIQUIDS#2 case. In particular, in the LIQUIDS#2 case, insufficient heterogeneous processing leads to a large and too-early deactivation of active chlorine into ClONO₂ at both latitudes. This in turn implies too little active chlorine available to deplete ozone and an underestimate of the rate of increase of HCl compared to the MLS observations by October (see below).

The premature deactivation into ClONO₂ in the LIQUIDS#2 case shuts off the ozone loss process by converting a great deal of the active chlorine back into the ClONO₂ reservoir starting in early September (e.g., day 240), before there is sufficient sunlight to drive substantial ozone loss. This behavior is related to the well-established concept of the ClONO₂ “collar” region [Toon *et al.*, 1989; see also Jaegle *et al.*, 1997]. A key finding of the present work is the application of the same chemical principles to identify the deactivation of active chlorine into ClONO₂ as a critical indicator of chemistry in regions poleward of the primary collar [see Chipperfield *et al.*, 1994, for an early and related study]. If deactivation into ClONO₂ occurs too early, then less chlorine is available to form HCl so that a linked indicator is a reduced rate of formation of HCl at later times in the season.

Arctic

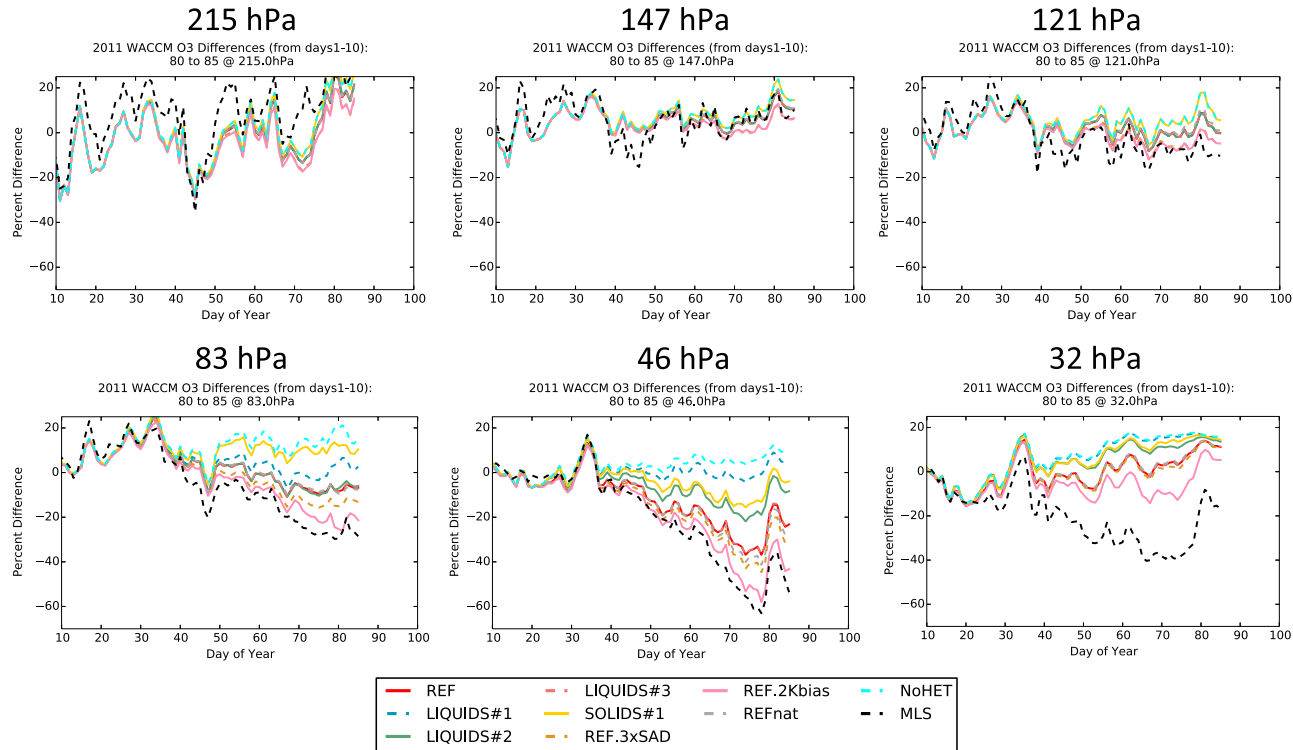


Figure 7. Seasonal evolution of percentage ozone changes at various pressure levels in the Arctic, averaged over 80°N to 85°N, for various model cases compared to MLS data, relative to days 1–10 for each case.

Observations of HCl and ClONO₂ are compared to the model results in more detail to further probe this behavior in Figures 9, 10 and S5, using MLS HCl, and MIPAS and ACE ClONO₂ measurements for latitudes 65–75°S and 75–85°S. Averaging over 10 degree bands is employed to better compare the data, particularly for ACE, which is an occultation instrument and has a limited number of measurements. Rates of change are shown for HCl in Figure 9. Prior to calculation of the tendencies, the zonal mean daily values were smoothed to remove higher frequency variability. This was done by applying a 15 day low-pass filter (a second-order Butterworth analog filter) to the time series [see Bandoro et al., 2014, and references therein]. Figure 9 shows that in the latitude band 65–75°S at this illustrative pressure level, the reference model matches the observed rate of change of HCl remarkably well, while the LIQUIDS#2 case falls below the observations, especially later in the ozone depletion season. Figure 9 thus illustrates that the rate of heterogeneous processing at temperatures below 192 K is critical to the evolution of HCl in this region and time of year (compare, e.g., the reference and LIQUIDS#2 for days 260–280 in Figure 9). The divergences of the observed and calculated rates of change of HCl for the two latitude bands are coincident with the growing disparities between the observed and calculated ozone losses in the same locations in the LIQUIDS#2 case, showing the usefulness of the rate of change of HCl as a chemical indicator, especially in Antarctica, where chemical perturbations are large.

Figures 10 and S5 compare the ranges of ClONO₂ abundances in the model to observations from MIPAS and ACE. Because of the sparseness of ACE ClONO₂ data, and because of its extremely large variability, the rates of change of observed ClONO₂ cannot be computed with fidelity. Midwinter measurements by MIPAS are also relatively sparse due to optical interference from thick polar stratospheric clouds. Absolute values of ClONO₂ from the model and from the two sets of satellite observations are therefore shown at the specific locations of the measurements as individually plotted points. The probability distributions of ClONO₂ from MIPAS data and model calculations for days 260–280 (when much of the ozone loss occurs) are also indicated. Results for the reference and LIQUIDS#2 cases compared to the NOHET case demonstrate that heterogeneous chemistry substantially

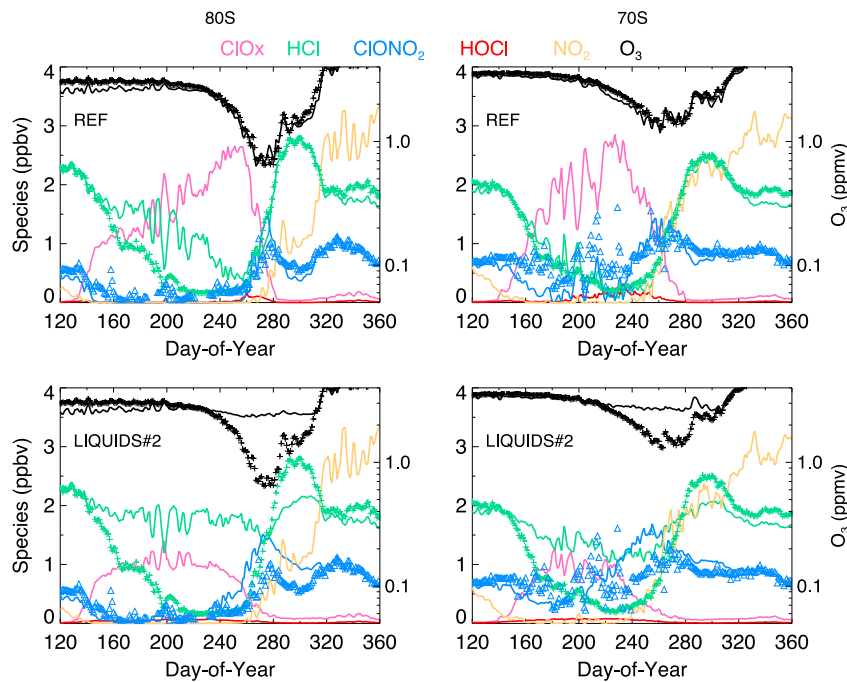


Figure 8. Evolution of zonally averaged chemical species at (left) 80°S and (right) 70°S near 30 hPa, for the (top) reference and (bottom) LIQUIDS#2 cases. Concentrations of ozone and HCl calculated by SD-WACCM (lines) are compared to MLS satellite data (crosses), and calculated abundances of related species are also indicated.

increases the variability of CIONO₂, in terms of both high and low extremes. The high extremes are linked to the rapid formation of CIONO₂ from enhanced ClO whenever NO₂ is available, while the low extremes reflect effective heterogeneous removal that subsequently drives CIONO₂ toward zero if heterogeneous chemistry is sufficiently rapid compared to the rate of reformation of CIONO₂. Variations linked to wave activity that lead to sporadic low and high temperatures, and transport air from sunlight to darkness and vice versa, strongly affect the CIONO₂ extremes. Arnone *et al.* [2012] show MIPAS observations of high CIONO₂ inside the edge of the Arctic vortex at times, similar to that presented here for Antarctica. It is important to note that the computed variability of the reference and LIQUIDS#2 model values decreases substantially as temperatures increase in the spring, again illustrating the fact that not only the abundance but also the variability of CIONO₂ is tightly linked to the rate of heterogeneous chemistry. MIPAS data display a similar marked decrease in variability after about day 275 in Figure 10. The LIQUIDS#2 case yields minimum CIONO₂ mixing ratios that are higher than their counterparts in ACE and MIPAS data (particularly after about day 250 in the latter), indicating a premature net recovery into the CIONO₂ reservoir (as suggested by the behavior of HCl in Figure 8 as well). At this latitude and altitude, the model reference case is able to match the extremes of both ACE and MIPAS observations of CIONO₂, although there is a clear bias in the reference model probability distribution function for days 260–280, where WACCM displays too many high values and too few low ones.

Figure S5 shows similar results as those of Figure 10 but for latitudes deeper in the vortex, 75–85°S, near 30 hPa, where the reference model values appear to overestimate somewhat both the high and low extremes during days 260–280. It is noticeable that the reference model is closer to the MIPAS range than the LIQUIDS#2 case throughout the season.

In summary, Figures 3, 4, 8, and 10 illustrate how the abundance, variability, and timing of the seasonal evolution of CIONO₂ provide a particularly sensitive indicator of chemical processing that is key to ozone depletion and its timing.

4.4. Transport and CIONO₂

Figure 11 examines the zonally averaged budget of CIONO₂ in the reference case for Antarctica, by showing the contributions of chemistry and advective transport to the calculated rate of change of CIONO₂ in SD-WACCM

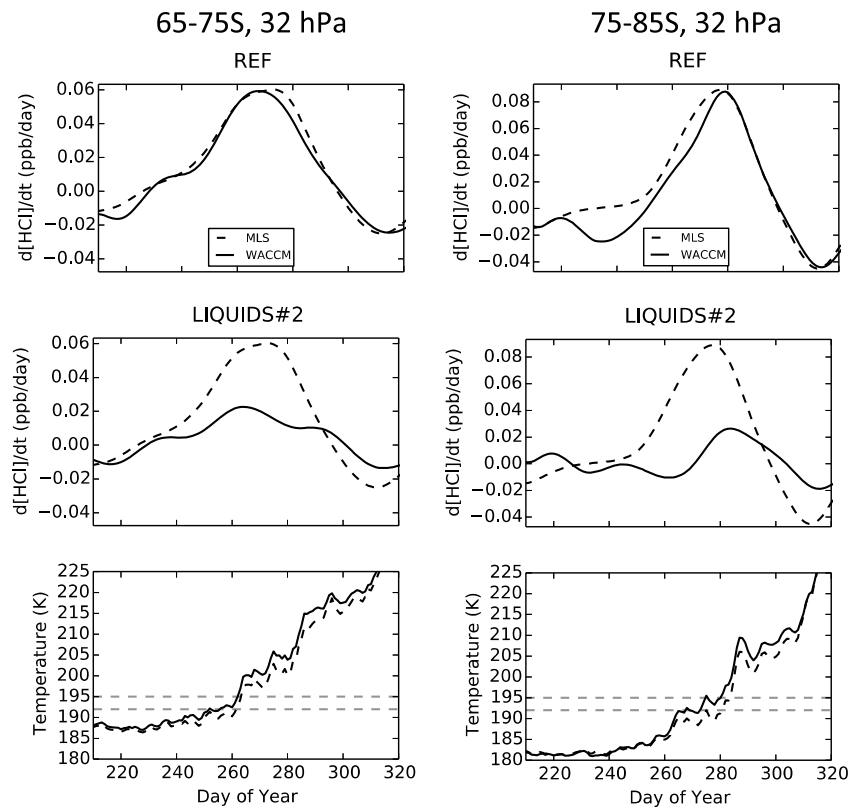


Figure 9. Rates of model-calculated changes of HCl (solid) versus time for the (top) reference and (middle) LIQUIDS#2 cases near 30 hPa, averaged (left) over 65–75°S and (right) 75–85°S compared to the corresponding MLS data (dashed). The temperatures from MERRA (solid) and MLS (dashed) are shown in the bottom panels. Horizontal dashed lines indicate 192 K and 195 K for reference.

as a function of latitude and day of the year near 60 hPa. ClONO₂ mixing ratios and the zonal wind speeds are also overlaid, showing the location of the ClONO₂ collar and the jet. A key feature of the middle panel in the figure is that ClONO₂ is transported effectively from lower latitudes (approximately 55°S to 65°S) to higher latitudes (approximately 65°S to 75°S), as indicated by the change from negative to positive tendencies from transport. In the higher latitude band, ClONO₂ is rapidly removed by heterogeneous processing in winter and spring, as reflected in the correspondingly negative chemical contribution to the budget. The time series of the peak (positive) advective and (negative) chemical tendencies in the band between 65°S and 75°S are shown in the bottom panel, indicating a high degree of cancellation between the two. Other metrics could have been used, but the three panels of this figure are one way to illustrate that the ClONO₂ that is supplied to higher latitudes by transport from lower latitudes is rapidly activated as it arrives. Thus, higher latitudes are linked chemically to lower latitudes, where rates of HNO₃ photolysis (and reaction with OH) are faster, and concentrations of NO_x and ClONO₂ are higher. This is especially significant in regions where the ClONO₂ abundance available at the start of polar night is insufficient to fully activate chlorine from HCl, since transport from lower, more sunlit regions can provide the NO_x needed for activation. Such linkage is a new finding of this paper, and it is likely to vary from one model to another depending upon transport. Figure 11 suggests that the core of the vortex poleward of about 75°S is considerably more isolated from these effects.

The time series shown in Figure 8 provides useful context for the results of Figure 11. Sporadic increases in ClONO₂ can be seen at 70°S, followed by rapid decreases (e.g., top right panel, days 180–240), and the figure shows that these play a key role in activating HCl at this location. In sharp contrast, at 80°S (top left panel), there is little or no midwinter ClONO₂, and HCl is not removed. Thus, in SD-WACCM driven by MERRA reanalysis fields, such transport is important at the edge of the vortex but rarely extends deeper than about 75°S so that the core of the vortex is isolated from this transport-induced boost to net activation. The lack of transport of ClONO₂ to higher latitudes is a possible explanation for insufficient

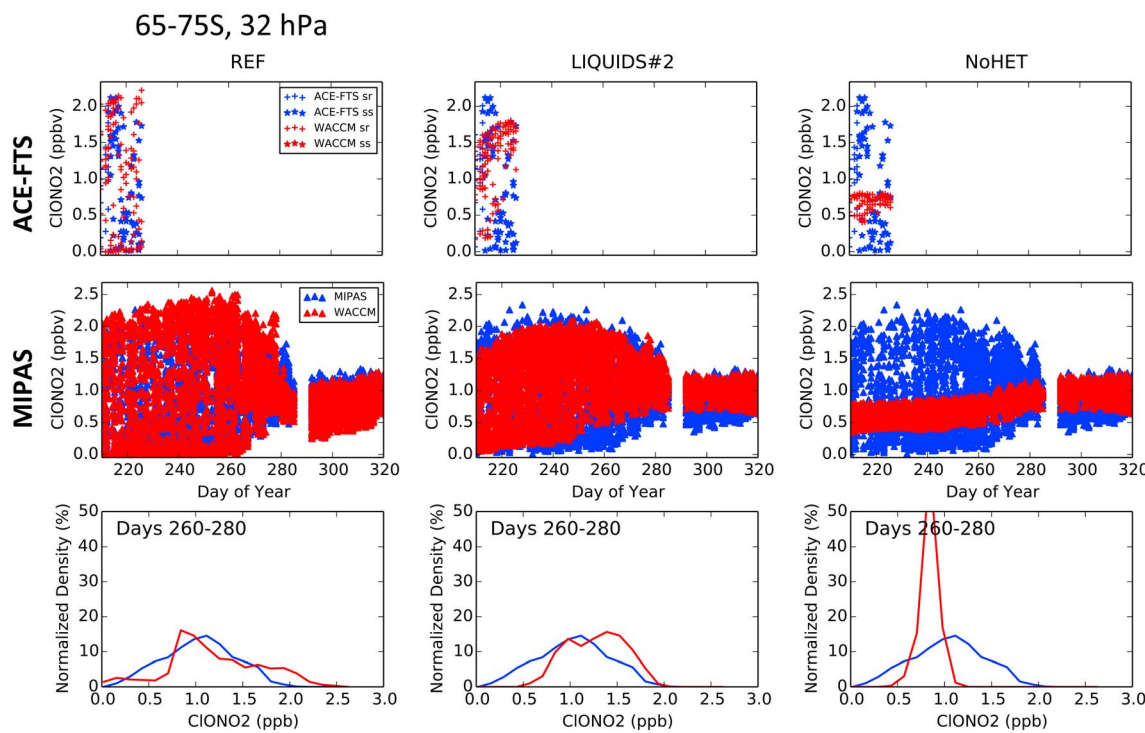


Figure 10. Abundances of CIONO₂ at 65–75°S near 30 hPa calculated in SD-WACCM compared to (top) ACE data (where “ss” and “sr” denote sunrise and sunset, respectively) and (middle) MIPAS data, for the (left) reference, (middle) LIQUIDS#2, and (right) no heterogeneous chemistry cases. SD-WACCM has been sampled at the locations and times of each individual satellite measurement, shown here as the cloud of points in each panel of the top two rows. The bottom panel shows probability distribution functions for CIONO₂ data calculated by WACCM (red) and observed by MIPAS (blue) for days 260–280.

removal of HCl in midwinter in the example shown for 80°S, near 30 hPa (Figure 8, left), in contrast to 70°S where the seasonal decline in SD-WACCM HCl closely tracks MLS observations (Figure 8, right).

5. Discussion and Conclusions

A series of test runs of polar ozone depletion chemistry have been presented using SD-WACCM, a version of WACCM4 constrained by observed meteorological fields from the MERRA reanalysis for 2011. Here we summarize five key conclusions of this study and discuss some important implications of the findings.

First, the occurrence of cold temperatures and polar stratospheric cloud chemistry at temperatures below 192 K is essential to produce in SD-WACCM substantial ozone losses similar to those observed in both hemispheres. Very limited ozone losses occur in SD-WACCM if liquid polar stratospheric clouds or binary aerosols alone are allowed to drive heterogeneous chemistry through reactivities and surface areas characteristic of temperatures of 192 K or warmer. Although there are some differences in detail (e.g., near 30 hPa in the Arctic), confidence in these results is bolstered by broad agreement of the temporal behavior of computed ozone and related species, including HNO₃, H₂O, CIONO₂, and HCl, at a wide range of pressure levels compared to data in both hemispheres.

Second, the tests show that the magnitude of calculated column ozone depletion in both polar regions is sensitive to small differences in temperature or to relatively small changes in volcanic sulfate aerosol surface areas. Both a cooling of 2 K, or a modest (factor of three) aerosol surface area increase (similar to what could result from relatively small volcanic eruptions), can increase total column ozone losses by 10–40 DU. It is interesting that such changes result in large relative differences in ozone loss near the Antarctic tropopause (Figure 2), where they can be expected to impact the influence of the ozone hole on Southern Hemisphere tropospheric climate. Further, these results are relevant to attempts to quantify ozone recovery as anthropogenic chlorine decays from the atmosphere, insofar as they indicate the accuracy to which temperatures and sulfate aerosol density changes need to be known if the role of changes of halogens is to be accounted for with sufficient precision to confidently attribute its influence.

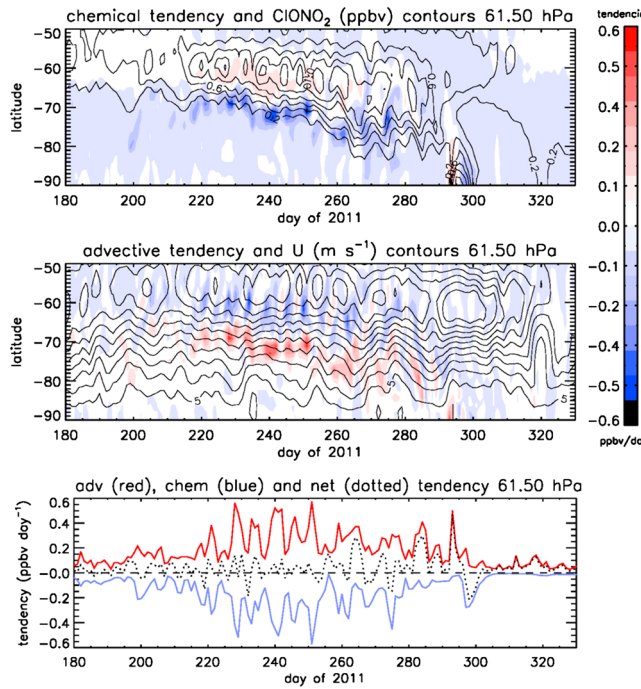


Figure 11. Factors influencing ClONO₂ in the Antarctic. All quantities are zonal averages at 61 hPa. (top) Rate of calculated ClONO₂ net chemical formation or destruction (color contours), along with ClONO₂ mixing ratios (overlaid in black lines). (middle) Advective transport (color contours) and zonal wind (overlaid in black lines). (bottom) Peak advective and chemical tendencies, and the net of the two terms.

particles in particular represents extrapolations rather than actual measurements below about 195 K [Shi *et al.*, 2001], the very temperatures shown to be critical for ozone losses here. Physical considerations and the detailed simulations presented suggest that solid particle impacts are important when the best representation of all particle types is considered, particularly at levels above about 18 km over Antarctica, where very cold temperatures allow for the frequent presence of water ice clouds. This model contains a simplified microphysics parameterization, and uncertainties in PSC composition, number densities, and variability should be considered, including such issues as parcel temperature histories, the supersaturation ratios required to form NAT or ice, and the effects of bimodal NAT particle distributions. Further laboratory measurements and a better understanding of particle composition and variability remain key research needs.

Fourth, the tests performed show that the springtime evolution of HCl and ClONO₂ are key indicators of ozone depletion chemistry. In particular, the presence of large amounts of ClONO₂ in early spring indicates that the efficacy of net heterogeneous processing (activation-deactivation) is insufficient to produce enough active chlorine to drive ozone loss. The early formation of ClONO₂ leads to reduced rates of production of HCl, and the rate of formation of HCl is hence also a key indicator of chemistry. MLS observations of the rate of formation of HCl at, for example, 70°S or 80°S near 30 hPa are in remarkable agreement with the reference model; ACE and MIPAS observations of ClONO₂ also show good general agreement at both latitudes in the reference case but agree less well if, for example, liquid chemistry is only allowed for temperatures above 192 K.

Fifth, analysis of the budget of ClONO₂ in SD-WACCM shows that transport of ClONO₂ from lower latitudes to higher latitudes in the Antarctic (i.e., from 55–65°S to 65–75°S) enhances the ClONO₂ available for reaction with HCl and hence net chlorine activation. Thus, transport links lower, more sunlit latitudes with more available NO_x to higher latitudes, boosting Antarctic heterogeneous processing.

In summary, we have evaluated the ability of SD-WACCM to simulate chlorine activation and deactivation in polar ozone depletion in both hemispheres and have probed the roles of different kinds of polar stratospheric clouds based on current chemical schemes. The model shows general consistency across a broad range of observed

Third, these results using SD-WACCM confirm numerous earlier studies suggesting that liquid PSC particles are sufficient to simulate nearly all of the ozone loss using current model chemistry. While this information can be useful for model parameterizations, it does not imply that solid particles play no role beyond their obvious importance for dehydration and denitrification in the real world. We have shown that results for each type of particle are not additive, and substantial ozone loss can be produced by each, although liquids are indeed generally more effective if both are present. A parameterization of the chemistry using supercooled liquid ternary PSCs alone can reproduce essentially all of the ozone loss in both hemispheres over all altitudes in WACCM as long as it is allowed to operate over the full range of temperatures, particularly those below 192 K. However, the kinetic rates of reactions on PSC surfaces (both NAT and liquids) are subject to significant uncertainties [Jet Propulsion Laboratory JPL, 2011]. Indeed, the current parameterization of heterogeneous rates on liquid

variables including ozone itself, the rate of formation of HCl, and ClONO₂ trends and variability, supporting the findings presented, despite some differences in detail. Analysis of the ClONO₂ and HCl seasonal variations, ClONO₂ variability, and transport terms across a range of state-of-the-art climate models such as the one shown here could provide further insight into outstanding questions such as the winter season decline of HCl in the core of the vortex.

Acknowledgments

We thank Meijong Park for help with the MLS data. D. E. Kinnison and S. Solomon were partially supported by NSF FESD grant OCE-1338814 and a grant from the NSF atmospheric chemistry division. The National Center for Atmospheric Research (NCAR) is sponsored by the U.S. National Science Foundation. WACCM is a component of the Community Earth System Model (CESM), which is supported by the National Science Foundation (NSF) and the Office of Science of the U.S. Department of Energy. Computing resources were provided by NCAR's Climate Simulation Laboratory, sponsored by NSF and other agencies. This research was enabled by the computational and storage resources of NCAR's Computational and Information System Laboratory (CISL). We are grateful to Michael Hopfner, Peter Bernath, and two anonymous referees for helpful comments and suggestions. We thank NASA Goddard Space Flight Center for the MERRA data (accessed freely online at <http://disc.sci.gsfc.nasa.gov/>). We also thank the MLS team for the constituent data used in this paper, freely available at <http://disc.sci.gsfc.nasa.gov/Aura/data holdings/MLS/>. We are grateful to the ACE team for their measurements, which are supported by the Canadian Space Agency (available via <http://www.ace.uwaterloo.ca/index.html>) and to the MIPAS team for their data (<https://www.imk-asf.kit.edu/english/308.php>). Model results shown in this paper are available on request to the WACCM liaison, Michael Mills (mmills@ucar.edu).

References

- Achtter, P., and M. Tesche (2014), Assessing lidar-based classification schemes for polar stratospheric clouds based on 16 years of measurements at Esrange, Sweden, *J. Geophys. Res. Atmos.*, **119**, 1386–1405, doi:10.1002/2013JD020355.
- Arfeuille, F., B. P. Luo, P. Heckendorn, D. Weisenstein, J. X. Sheng, E. Rozanov, M. Schraner, S. Brönnimann, L. W. Thomason, and T. Peter (2013), Modeling the stratospheric warming following the Mt. Pinatubo eruption: Uncertainties in aerosol extinction, *Atmos. Chem. Phys.*, **13**, 11,221–11,234, doi:10.5194/acp-13-11221-2013.
- Arnone, E., E. Castelli, E. Papandrea, M. Carlotti, and B. M. Dinelli (2012), Extreme ozone depletion in the 2010–2011 Arctic winter stratosphere as observed by MIPAS/ENVISAT using a 2-D tomographic approach, *Atmos. Chem. Phys.*, **12**, 9149–9165.
- Bandoro, J., S. Solomon, A. Donohoe, D. W. J. Thompson, and B. Santer (2014), Influences of the Antarctic ozone hole on Southern Hemispheric summer climate change, *J. Clim.*, **27**, 6245–6264.
- Biele, J., A. Tsias, B. Luo, K. Carslaw, R. Neuber, G. Beyerle, and T. Peter (2001), Non-equilibrium coexistence of solid and liquid particles in Arctic stratospheric clouds, *J. Geophys. Res.*, **106**, 22,991–23,007, doi:10.1029/2001JD900188.
- Brakebusch, M., C. E. Randall, D. E. Kinnison, S. Tilmes, M. L. Santee, and G. L. Manney (2013), Evaluation of Whole Atmosphere Community Climate Model simulations of ozone during Arctic winter 2004–2005, *J. Geophys. Res. Atmos.*, **118**, 2673–2688, doi:10.1002/jgrd.50226.
- Bregman, A., M. van den Broek, K. S. Carslaw, R. Mueller, T. Peter, M. P. Scheele, and J. Lelieveld (1997), Ozone depletion in the late winter lower Arctic stratosphere: Observations and model results, *J. Geophys. Res.*, **102**, 10,815–10,828, doi:10.1029/97JD00006.
- Carslaw, K. S., B. P. Luo, S. L. Clegg, T. Peter, P. Brimblecombe, and P. J. Crutzen (1994), Stratospheric aerosol growth and HNO₃ gas phase depletion from coupled HNO₃ and water uptake by liquid particles, *Geophys. Res. Lett.*, **21**, 2479–2482, doi:10.1029/94GL02799.
- Carslaw, K. S., T. Peter, and R. Mueller (1997), Uncertainties in reactive uptake coefficients for solid stratospheric particles—2. Effect on ozone depletion, *Geophys. Res. Lett.*, **24**, 1747–1750, doi:10.1029/97GL01684.
- Chipperfield, M. P., D. Cariolle, and P. Simon (1994), A 3D transport model study of chlorine activation during EASOE, *Geophys. Res. Lett.*, **21**, 1467–1470, doi:10.1029/93GL01679.
- Considine, D. B., A. R. Douglass, P. S. Connell, D. E. Kinnison, and D. A. Rotman (2000), A polar stratospheric cloud parameterization for the three dimensional model of the global modeling initiative and its response to stratospheric aircraft, *J. Geophys. Res.*, **105**, 3955–3975, doi:10.1029/1999JD900932.
- Davies, S. M. P., et al. (2002), Modeling the effect of denitrification on Arctic ozone depletion during winter 1999/2000, *J. Geophys. Res.*, **108**(D5), 8322, doi:10.1029/2001JD000445.
- Deshler, T., B. J. Johnson, and W. R. Rozier (1994), Changes in the character of polar stratospheric clouds over Antarctica in 1992 due to the Pinatubo volcanic aerosol, *Geophys. Res. Lett.*, **21**, 273–276, doi:10.1029/94GL00072.
- Douglass, A. R., M. R. Schoeberl, R. S. Stolarski, J. W. Waters, J. M. Russell III, A. E. Roche, and S. T. Massie (1995), Interhemispheric differences in springtime production of HCl and ClONO₂ in the polar vortices, *J. Geophys. Res.*, **100**, 13,967–13,978, doi:10.1029/95JD00698.
- Drdla, K., and R. Mueller (2012), Temperature thresholds for chlorine activation and ozone loss in the polar stratosphere, *Ann. Geophys.*, **30**, 1055–1073, doi:10.5194/angeo-30-1055-2012.
- Eyring, V., T. G. Shepherd, and D. W. Waugh (Eds.) (2010), SPARC report on the evaluation of chemistry-climate models, *SPARC Rep. 5, WRCP-132, WMO-TD 1526*, World Meteorol. Organ., Geneva, Switzerland.
- Fahey, D. W., et al. (2001), The detection of large HNO₃-containing particles in the winter Arctic stratosphere, *Science*, **291**, 1026–1031, doi:10.1126/science.1057265.
- Feng, W., M. P. Chipperfield, S. Davies, G. W. Mann, K. S. Carslaw, S. Dhomse, L. Harvey, C. Randall, and M. L. Santee (2011), Modelling the effect of denitrification on polar ozone depletion for Arctic winter 2004/2005, *Atmos. Chem. Phys.*, **11**, 6559–6573.
- Hanson, D., and K. Mauersberger (1988), Laboratory studies of the nitric acid trihydrate: Implications for the south polar stratosphere, *Geophys. Res. Lett.*, **15**, 855–858, doi:10.1029/GL015i008p00855.
- Hanson, D. R. (2003), Reactivity of BrONO₂ and HOBr on sulfuric acid solutions at low temperatures, *J. Geophys. Res.*, **108**(D8), 4239, doi:10.1029/2002JD002519.
- Hanson, D. R., A. R. Ravishankara, and S. Solomon (1994), Heterogeneous reactions in sulfuric acid aerosols: A framework for model calculations, *J. Geophys. Res.*, **99**, 3615–3629, doi:10.1029/93JD02932.
- Hanson, D. R., A. R. Ravishankara, and E. R. Lovejoy (1996), Reaction of BrONO₂ with H₂O on submicron sulfuric acid aerosol and the implications for the lower stratosphere, *J. Geophys. Res.*, **101**, 9063–9069, doi:10.1029/96JD00347.
- Hoyle, C. R., I. Engel, B. P. Luo, M. C. Pitts, L. R. Poole, J.-U. Grooß, and T. Peter (2013), Heterogeneous formation of polar stratospheric clouds—Part 1: Nucleation of nitric acid trihydrate (NAT), *Atmos. Chem. Phys.*, **13**, 9577–9595, doi:10.5194/acp-13-9577-2013.
- Jaegle, L., et al. (1997), Evolution and stoichiometry of heterogeneous processing in the Antarctic stratosphere, *J. Geophys. Res.*, **102**, 13,235–13,253, doi:10.1029/97JD00935.
- Jet Propulsion Laboratory JPL (2011), *Chemical Kinetics and Photochemical Data for Use in Atmospheric Studies*, vol. 15, JPL Publication, 06-2, Jet Propulsion Lab., Pasadena.
- Kinnison, D. E., et al. (2007), Sensitivity of chemical tracers to meteorological parameters in the MOZART-3 chemical transport model, *J. Geophys. Res.*, **112**, D20302, doi:10.1029/2006JD007879.
- Koop, T., U. M. Biermann, W. Raber, B. P. Luo, P. J. Crutzen, and T. Peter (1995), Do stratospheric aerosol droplets freeze above the ice frost point?, *Geophys. Res. Lett.*, **22**, 917–920, doi:10.1029/95GL00814.
- Kunz, A., L. Pan, P. Konopka, D. E. Kinnison, and S. Tilmes (2011), Chemical and dynamical discontinuity at the extratropical tropopause based on START08 and WACCM analysis, *J. Geophys. Res.*, **116**, D24302, doi:10.1029/2011JD016686.
- Kuttippurath, J., S. Godin-Beekmann, F. Lefèvre, G. Nikulin, M. L. Santee, and L. Froidevaux (2012), Record-breaking ozone loss in the Arctic winter 2010/2011: Comparison with 1996/1997, *Atmos. Chem. Phys.*, **12**, 7073–7085, doi:10.5194/acp-12-7073-2012.

- Lamarque, J.-F., et al. (2012), CAM-chem: Description and evaluation of interactive atmospheric chemistry in the Community Earth System Model, *Geosci. Model Dev.*, 5, 369–411, doi:10.5194/gmd-5-369-2012.
- Larsen, N., B. M. Knudsen, J. M. Rosen, N. T. Kjome, R. Neuber, and E. Kyro (1997), Temperature histories in liquid and solid polar stratospheric cloud formation, *J. Geophys. Res.*, 102, 23,305–23,517, doi:10.1029/97JD01666.
- Manney, G. L., et al. (2011), Unprecedented Arctic ozone loss in 2011, *Nature*, 478, 469–475, doi:10.1038/nature10556.
- Marsh, D. R. M. J., D. E. Mills, J. F. Kinnison, N. C. Lamarque, and L. M. Polvani (2013), Climate change from 1850 to 2005 simulated in CESM1 (WACCM), *J. Clim.*, 26, 7372–7391, doi:10.1175/JCLI-D-12-00558.1.
- Meilinger, S., T. Koop, B. P. Luo, T. Huthwelker, K. S. Carslaw, U. Krieger, P. J. Crutzen, and T. Peter (1995), Size-dependent stratospheric droplet composition in mesoscale temperature fluctuations and their potential role in PSC freezing, *Geophys. Res. Lett.*, 22, 3031–3034, doi:10.1029/95GL03056.
- Neale, R. B., et al. (2010), Description of the NCAR Community Atmosphere Model (CAM4.0), NCAR Technical Note, TN-485+STR. [Available at <http://www.cesm.ucar.edu/models/cesm1.0/cam>.]
- Neale, R., J. Richter, S. Park, P. Lauritzen, S. Vavrus, P. Rasch, and M. Zhang (2013), The mean climate of the Community Atmosphere Model (CAM4) in forced SST and fully coupled experiments, *J. Clim.*, 26, 5150–5168.
- Peter, T., and J. U. Grooß (2012), Polar stratospheric clouds and sulfate aerosol particles: Microphysics, denitrification and heterogeneous chemistry, in *Stratospheric Ozone Depletion and Climate Change*, chap. 4, pp. 108–144, R. Soc. of Chem., Cambridge, U. K., doi:10.1039/9781849733182-00108.
- Peter, T., C. Brühl, and P. J. Crutzen (1991), Increase in the PSC-formation probability caused by high-flying aircraft, *Geophys. Res. Lett.*, 18, 1465–1468, doi:10.1029/91GL01562.
- Pitts, M. C., L. R. Poole, and L. W. Thomason (2009), CALIPSO polar stratospheric cloud observations: Second-generation detection algorithm and composition discrimination, *Atmos. Chem. Phys.*, 9, 7577–7589.
- Pitts, M. C., L. R. Poole, A. Lambert, and L. W. Thomason (2013), An assessment of CALIOP polar stratospheric cloud composition classification, *Atmos. Chem. Phys.*, 13, 2975–2988, doi:10.5194/acp-13-2975-2013.
- Portmann, R. W., S. Solomon, R. R. Garcia, L. W. Thomason, L. R. Poole, and M. P. McCormick (1996), Role of aerosol variations in anthropogenic ozone depletion in the polar regions, *J. Geophys. Res.*, 101(D17), 22,991–23,006, doi:10.1029/96JD02608.
- Rex, M., R. J. Salawitch, P. von der Gathen, N. R. P. Harris, M. P. Chipperfield, and B. Naujokat (2004), Arctic ozone loss and climate change, *Geophys. Res. Lett.*, 31, L04116, doi:10.1029/2003GL018844.
- Ravishankara, A. R., and D. R. Hanson (1996), Differences in the reactivity of type I polar stratospheric clouds depending on their phase, *J. Geophys. Res.*, 101(D2), 3885–3890, doi:10.1029/95JD03009.
- Ridley, D. A., et al. (2014), Total volcanic stratospheric aerosol optical depths and implications for global climate change, *Geophys. Res. Lett.*, 41, 7763–7769, doi:10.1002/2014GL061541.
- Rienecker, M. M., et al. (2011), MERRA: NASA's Modern-Era Retrospective Analysis for Research and Applications, *J. Clim.*, 24, 3624–3648, doi:10.1175/JCLI-D-11-00015.1.
- Shi, Q., J. T. Jayne, C. E. Kolb, D. R. Worsnop, and P. Davidovits (2001), Kinetic model for reaction of ClONO₂ with H₂O and HCl and HOCl with HCl in sulfuric acid solutions, *J. Geophys. Res.*, 106(D20), 24,259–24,274, doi:10.1029/2000JD000181.
- Sinnhuber, B. M., G. Stiller, R. Ruhnke, T. von Clarmann, S. Kellmann, and J. Aschmann (2011), Arctic winter 2010/2011 at the brink of an ozone hole, *Geophys. Res. Lett.*, 38, L24814, doi:10.1029/2011GL049784.
- Solomon, S. (1999), Stratospheric ozone depletion: A review of concepts and history, *Rev. Geophys.*, 37, 275–316, doi:10.1029/1999RG900008.
- Solomon, S., R. R. Garcia, F. S. Rowland, and D. J. Wuebbles (1986), On the depletion of Antarctic ozone, *Nature*, 321, 755–758.
- Tabazadeh, A., R. P. Turco, K. Drdla, M. Z. Jacobson, and O. B. Toon (1994a), A study of type I polar stratospheric cloud formation, *Geophys. Res. Lett.*, 21, 1619–1622, doi:10.1029/94GL01368.
- Tabazadeh, A., R. P. Turco, and M. Z. Jacobson (1994b), A model for studying the composition and chemical effects of stratospheric aerosols, *J. Geophys. Res.*, 99(D6), 12,897–12,914, doi:10.1029/94JD00820.
- Toon, G. C., C. B. Farmer, L. L. Lowes, P. W. Schaper, J.-F. Blavier, and R. H. Norton (1989), Infrared aircraft measurements of stratospheric composition over Antarctica during September 1987, *J. Geophys. Res.*, 94, 16,571–16,596, doi:10.1029/JD094iD14p16571.
- Toon, O. B., P. Hamill, R. P. Turco, and J. Pinto (1986), Condensation of NO₃ and HCl in the winter polar stratosphere, *Geophys. Res. Lett.*, 13, 1284–1287, doi:10.1029/GL013i012p01284.
- Tsias, A., et al. (1999), Aircraft lidar observations of an enhanced type Ia polar stratospheric cloud during APE-POLECAT, *J. Geophys. Res.*, 104, 23,961–23,969, doi:10.1029/1998JD100055.
- Van den Broek, M. M., P. A. Bregman, and J. Lelieveld (2000), Model study of chlorine activation and ozone loss during the 1996/7 winter, *J. Geophys. Res.*, 105, 28,961–28,977, doi:10.1029/2000JD900294.
- Vernier, J.-P., et al. (2011), Major influence of tropical volcanic eruptions on the stratospheric aerosol layer during the last decade, *Geophys. Res. Lett.*, 38, L12807, doi:10.1029/2011GL047563.
- Waibel, A. E., T. Peter, K. S. Carslaw, H. Oelhaf, G. Wetzel, P. J. Crutzen, U. Poeschl, A. Tsias, E. Reimer, and H. Fischer (1999), Arctic ozone loss due to denitrification, *Science*, 283, 2064–2069, doi:10.1126/science.283.5410.2064.
- Wegner, T., D. E. Kinnison, R. R. Garcia, S. Madronich, and S. Solomon (2013), Simulation of polar stratospheric clouds in the specified dynamics version of the Whole Atmosphere Community Climate Model, *J. Geophys. Res. Atmos.*, 118, 5105–5110, doi:10.1002/jgrd.50443.
- Wohltmann, I., et al. (2013), Uncertainties in modelling heterogeneous chemistry and Arctic ozone depletion in the winter 2009/2010, *Atmos. Chem. Phys.*, 13, 3909–3929, doi:10.5194/acp-13-3909-2013.



Journal of Geophysical Research - Atmospheres

Supporting Information for

Simulation of Polar Ozone Depletion: An Update

Susan Solomon¹, Doug Kinnison², Justin Bandoro¹, Rolando Garcia²

¹Department of Earth, Atmospheric, and Planetary Sciences, Massachusetts Institute of Technology, Cambridge, MA 02139

²Atmospheric Chemistry Division, National Center for Atmospheric Research, Boulder, CO 80307

Contents of this file

Figures S1 to S5

Introduction

In this supplement, we present complementary figures to those in the main text. The model's ability to simulate dehydration and denitrification is illustrated in Figure S1. Figures S2-S5 present information similar to that shown in the main text, and complement figures in the main text with additional cases, latitudes or pressure levels. See main text for further details.

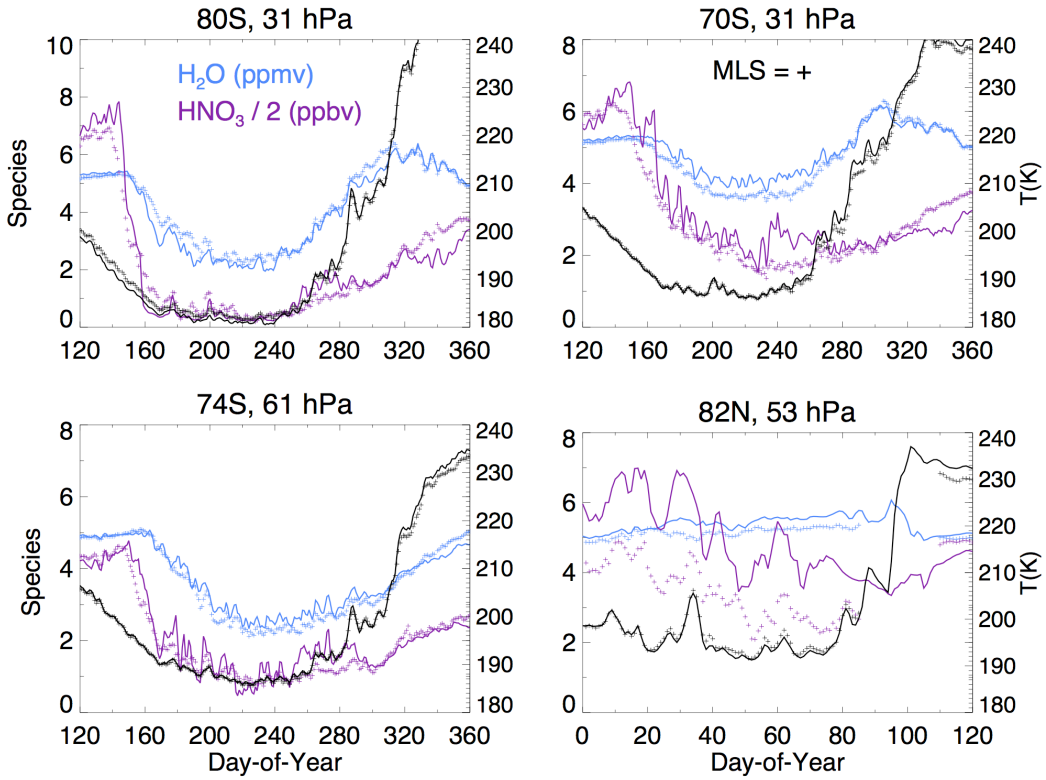


Figure S1. Comparisons of observed and modelled seasonal evolution of temperature (black), H₂O (cyan) and HNO₃ (purple) from MLS (shown as points) and from SD-WACCM (shown as lines) at several illustrative latitudes and pressure levels.

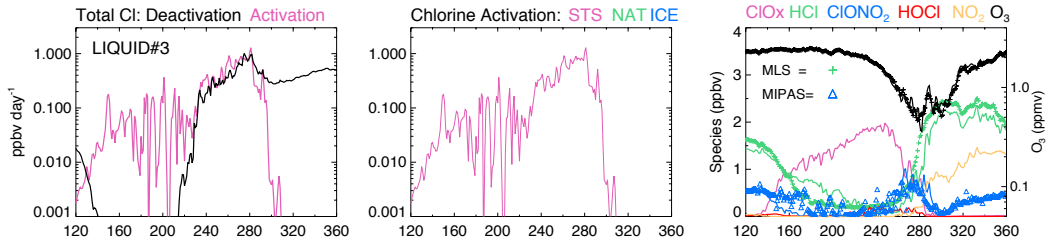


Figure S2. Key chemical processes and constituents at 74°S (zonally averaged), 61 mbar. Rates of activation of chlorine (driven by the heterogeneous reactions on liquid particles, NAT, and ice as in Table 1) and rates of deactivation (through conversion to ClONO₂ and HCl) are shown for the liquids#3 case. Concentrations of ozone, HCl and ClONO₂ calculated by SD-WACCM are compared to MLS and MIPAS satellite data in the right panels, where calculated abundances of related species are also indicated.

Antarctic

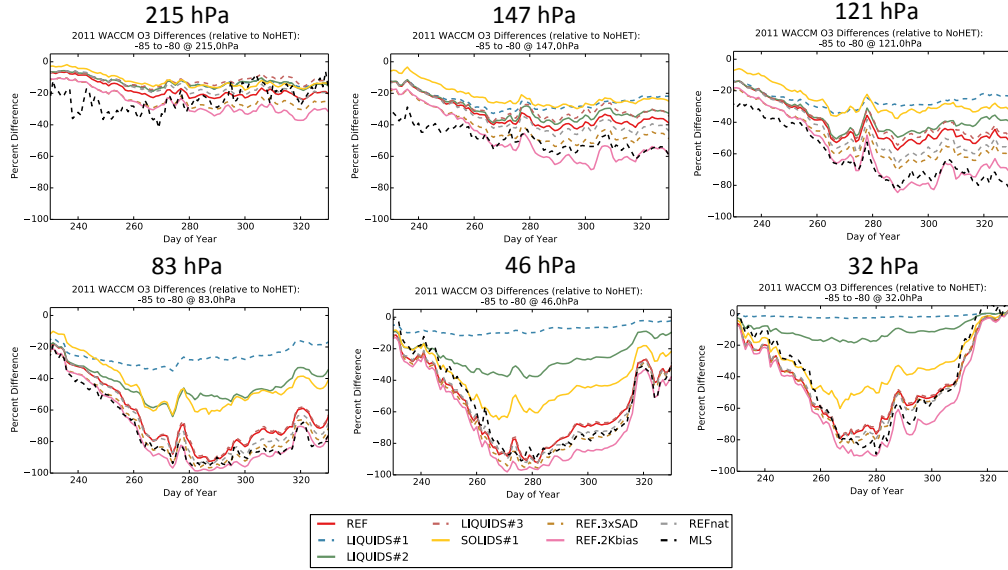


Figure S3. Seasonal evolution of percentage ozone changes at various pressure levels in the Antarctic, averaged over 80S to 85S, for various model cases, relative to the NOHET case for each day.

Arctic

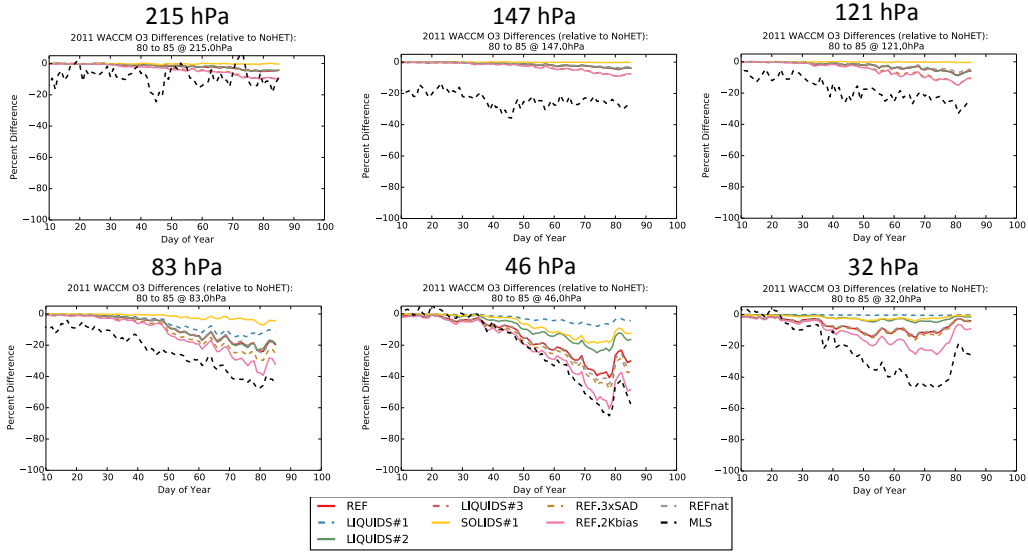


Figure S4. Seasonal evolution of percentage ozone changes at various pressure levels in the Arctic, averaged over 80S to 85S, for various model cases, relative to the NOHET case for each day.

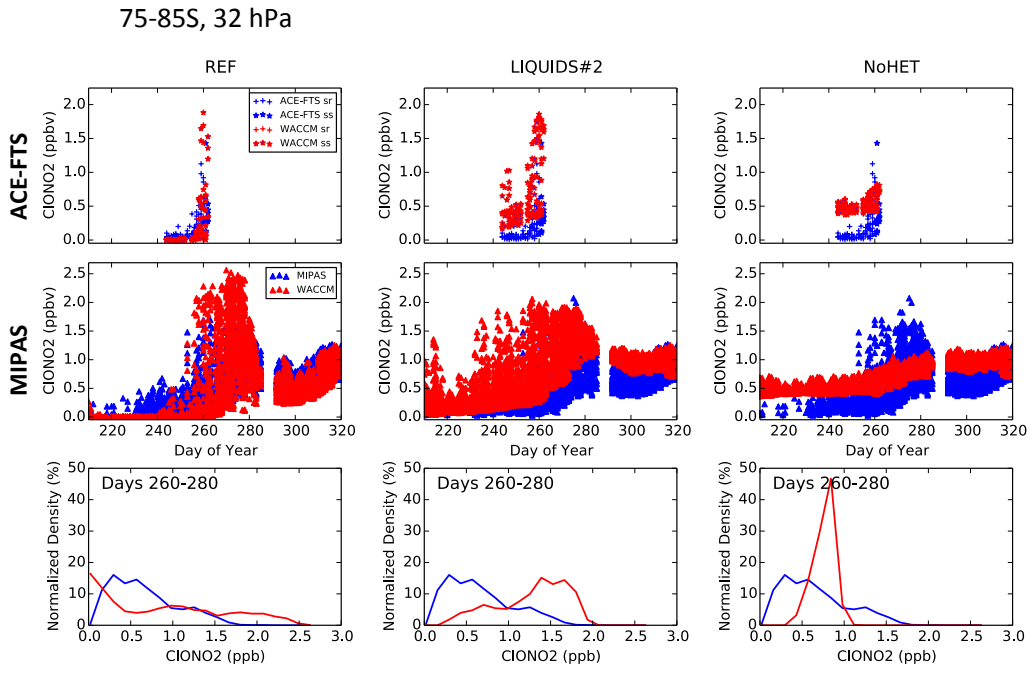


Figure S5. Abundances of CIONO₂ at 75-85S near 30 mbar calculated in SD-WACCM compared to ACE data (top row, where “ss” and “sr” denote sunrise and sunset, respectively) and MIPAS data (middle row), for the reference (left), liquids#2 (middle) and no heterogeneous chemistry cases (right). SD-WACCM has been sampled at the locations and times of each individual satellite measurement, shown here as the cloud of points in each panel of the top two rows. The bottom panel shows probability distribution functions for CIONO₂ data calculated by WACCM (red) and observed by MIPAS (blue) for days 260-280.